

# Technical Appendix: Functional Connectomes of Neural Networks

## Baseline Methods

We explored six baseline methods. Four of these methods employ the k-medoids algorithm with the following distances and kernels: bottleneck distance (BD), Wasserstein distance (WD), sliced Wasserstein kernel (SWK) (Carriere, Cuturi, and Oudot 2017), and heat kernel (HK) (Reininghaus et al. 2015). These methods use the weighted adjacency matrices, also referred to as functional connectomes  $C$ , as input. From these, we compute persistence diagrams of cycles ( $H_1$ ) using the `rips` (Tralie, Saul, and Bar-On 2018) package. Since `rips` expects distance matrices  $D$  as input, the functional connectomes are converted to distance matrices via the formula  $D = \sqrt{1 - C}$  (Songdechakruiwut and Chung 2023). This transformation captures the inverse relationship between correlation and distance while preserving the symmetry and triangle inequality of the distance matrix. We then calculate pairwise distance from persistence diagrams using the `persim` (Saul and Tralie 2021) package and perform k-medoids clustering. The default settings are used in both `rips` and `persim`. The k-medoids algorithm is implemented in `sklearn_extra` (scikit-learn extra 2020) with the settings of `metric="precomputed", init="random", method="pam"`.

The other two use a k-means clustering algorithm on persistence image (PI) (Adams et al. 2017) vectorization and on the vectorization of entries below the main diagonal of the adjacency (Adj), respectively. Persistence Images are obtained from persistence diagrams using `PersistenceImager` in `persim` with settings `birth_range=(0, 1), pers_range=(0, 1), pixel_size=0.05`, which convert persistence diagrams to persistence images of  $20 \times 20$  resolution. These images are then flattened into vectors. Euclidean distances between these vectors are computed to perform k-means clustering. K-means in `sklearn` (Pedregosa et al. 2011) is implemented with the settings of `init="random", n_init=1`. `traditional_clustering_pipeline.py` provides more details on the implementation of BD, WD, SWK, HK, PI, and `clustering_pipeline.py` provides more detail on the implementation of Adj.

## Dataset

In order to investigate the functional behavior of neural networks, we performed our analyses on the MNIST (Le-Cun et al. 1998), Fashion-MNIST (Xiao, Rasul, and Vollgraf 2017), and CIFAR-10 (Krizhevsky, Hinton et al. 2009) datasets. These datasets are widely used in the context of image classification tasks. The datasets are directly obtained from `torchvision` (TorchVision 2016). The detailed implementation of dataset loading is available in the code as a part of the `loading_pipeline.py` script.

The MNIST dataset comprises grayscale images of handwritten digits from 0 to 9. Each image has a centered digit with a resolution of  $28 \times 28$ . The training set contains 60,000 examples, and the test set contains 10,000 examples. The Fashion-MNIST dataset consists of grayscale images of fashion items. The images are categorized into ten classes: T-shirt/top, trousers, pullover, dress, coat, sandal, shirt, sneaker, bag, and ankle boot. The dataset shares the same number of training and testing examples and the same image resolution as MNIST. The CIFAR-10 dataset consists of color images of ten classes of common objects and animals, including airplane, automobile, bird, cat, deer, dog, frog, horse, ship, and truck. Each image has three color channels with a resolution of  $32 \times 32$ . The training set contains 50,000 images, and the test set contains 10,000 images.

In our studies, each dataset is split into training and functional datasets. The training dataset is used to train networks, and the functional dataset is used to produce functional connectomes. We used one-sixth of the original training data as the functional dataset. The implementations slightly differ in the two studies. In the first study, a random split is implemented using `randperm` in `torch` (Paszke et al. 2019). In the second study, we implemented `StratifiedShuffleSplit` in `sklearn` in order to maintain the same distribution of classes in training and functional datasets. Both studies had a fixed seed for reproducibility. More details on the design of the two studies are described in Section 3 of the main text.

## Hyperparameter Tuning

Hyperparameter tuning selects the combination of hyperparameters that yields the most optimal performance for a model. It ensures the model is learning effectively. In our studies, we perform hyperparameter tuning using  $k$ -fold

cross-validation. The training dataset is divided into five equal parts, where four parts are used for training, and one part is used for testing. By comparing the test accuracies of all hyperparameter combinations, the optimal set of hyperparameter combinations is determined. The detailed implementation of  $k$ -fold cross-validation is available in the code as a part of the `training_pipeline.py` script.

The tuning process focused on four key hyperparameters, including the training epoch number ( $e$ ), the negative slope coefficient ( $\alpha$ ) in the leaky ReLU activation function (Maas et al. 2013), the regularization strength ( $\lambda$ ) in  $L^2$  regularization (Hoerl and Kennard 1970), and the dropout rate ( $d$ ) (Srivastava et al. 2014). Specifically,  $e$  represents the number of training iterations,  $\alpha$  represents the negative slope coefficient applied to the negative input in Leaky ReLU,  $\lambda$  represents the regularization rate that penalizes large weights  $w_i$  in  $\text{Loss} = \text{Error}(y, \hat{y}) + \lambda \sum_{i=1}^N w_i^2$  for  $L^2$  regularization, and  $d$  represents the probability of dropping out each neuron. The hyperparameters are given choices as follows.

| Hyperparameter             | Choices                    |
|----------------------------|----------------------------|
| $e$ (training epoch)       | 20, 30, 40                 |
| $\alpha$ (LReLU slope)     | 0.01, 0.1                  |
| $\lambda$ ( $L^2$ penalty) | 0.0001, 0.001, 0.005, 0.01 |
| $d$ (dropout rate)         | 0.1, 0.2, 0.3, 0.4         |

Table 1: Hyperparameters Grid Search Choices

We adopted a grid search approach to search for the optimal model over predefined hyperparameters. First, the Cartesian product of different hyperparameters is calculated to define the grid search space. Then, models with sets of hyperparameter values are evaluated and compared based on the test accuracies. In the case where hyperparameters are shared across experiments, identical choices are offered in the grid search space. Since we are interested in the influence of regularization strategies in comparison to vanilla, these strategies are implemented separately in experiments where no two strategies are applied together. More details on hyperparameters and grid search can be found in `training_pipeline.py` and scripts of individual experiments.

There was a slight variation in how the training dataset was partitioned between the two studies. In the first study, we performed cluster analysis on regularization types with stimuli from all predefined classes. Thus,  $k$ -fold with  $k = 5$  in `torch` was implemented to partition training data into folds completely randomly. In the second study, we performed cluster analysis on stimuli from specific classes. A stratified version of  $k$ -fold in `sklearn` was implemented so that it was randomly partitioned within each predefined class. This approach ensured that each fold maintained the same distribution of predefined classes.

## Additional Results of Study 1

In Study 1, we examined the influence of different regularization strategies on functional mechanisms, including batch normalization (Ioffe and Szegedy 2015), dropout, and  $L^2$ .

For each strategy and the control group *vanilla*, we trained 20 neural networks. Then, we inputted the functional dataset into each trained network and extracted a functional connectome from it. This process resulted in 20 connectomes per regularization strategy. We then conducted cluster analysis on these functional connectomes with varying topological weights  $\lambda$  (Songdechakraiut et al. 2022).  $\lambda$  represents the degree to which topological information influences the interpolation between Adj and Top. When  $\lambda = 0$ , the algorithm only utilizes geometric information, representing the method Adj. When  $\lambda = 1$ , the method only uses topological information, corresponding to the method Top.

The clustering performance was assessed using purity scores, a value ranging from 0 to 1 (Manning, Raghavan, and Schütze 2008). A purity score of 1 indicates perfect clustering alignment within clusters, while a random assignment of clusters yields purity scores close to  $\frac{1}{N}$ , where  $N$  is the number of clusters. The results in Figures 1 to 4 present the comparison of clustering performance across datasets with varying topological weight  $\lambda$ . Each figure corresponds to a separate clustering task: Figure 1 displays the clustering performance when clustering connectomes from all regularization strategies and vanilla together, and Figures 2 to 4 show the clustering performances of clustering connectomes from vanilla and a regularization strategy (batch normalization, dropout, and  $L^2$ ). For each clustering task, we performed 20 trials. The data points represent the mean purity scores across these trials, and the error bars at each point represent the standard deviations of the purity scores.

Across Figures 1 to 4, we observe an overall positive correlation between the purity scores and the topological weight  $\lambda$ . Generally, incorporating more topological information tends to improve clustering performance. At the left end of the figures, where  $\lambda = 0$ , most purity scores for Adj are close to those expected from random cluster assignments. At the right end of  $\lambda = 1$ , the purity scores are significantly higher across all experiments, with many approaching 1. In every clustering task, the highest purity scores occur at  $\lambda = 1$ , indicating optimal performance. This suggests that topological information captured by Top is effective in distinguishing the functional differences between regularization techniques.

## Generalization to Convolutional Layer

In addition to constructing connectomes for fully connected layers in feedforward networks, we extended our framework to convolutional layers. In previous experiments on fully connected layers, we concatenated the output of individual neurons for all data points into a functional vector. For convolutional operation, the unit to collect activation becomes windows over a matrix, and the output of individual windows becomes activation maps. We adopted the approach to first apply an aggregation function to the activation maps, and then to concatenate the activation values from each window into a functional vector. In the context of convolutional layers, the functional vector represents the functional signals from specific regions of the image.

With this construction of functional connectomes, we performed connectome analysis on two types of architecture:

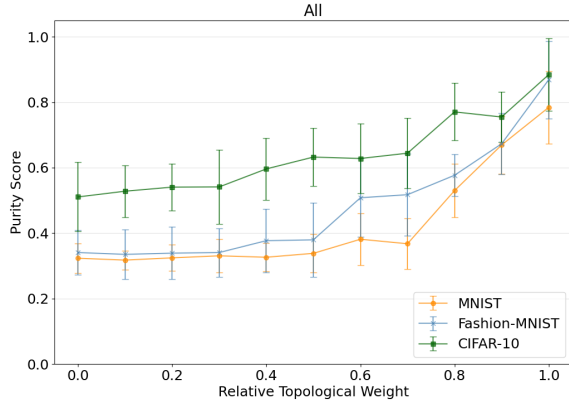


Figure 1: Purity scores of clustering connectomes of all regularization strategies into four clusters. The variation of relative topological weight  $\lambda$  in the clustering method influences its performance.

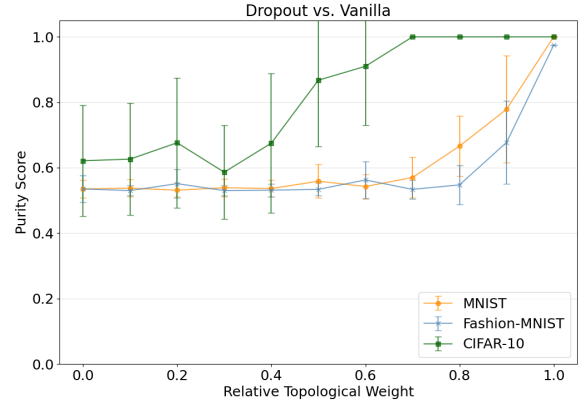


Figure 3: Purity scores of clustering connectomes of dropout and vanilla into two clusters with varying topological weight  $\lambda$ .

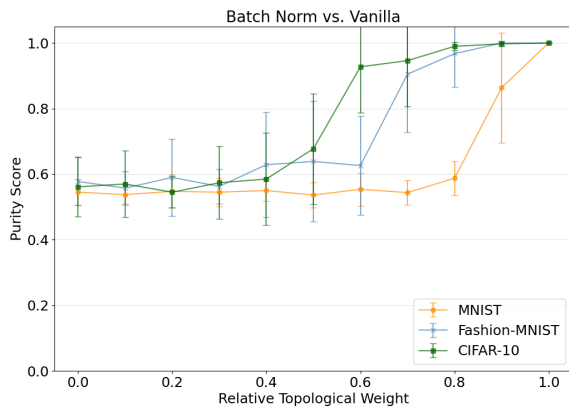


Figure 2: Purity scores of clustering connectomes of batch normalization and vanilla into two clusters with varying topological weight  $\lambda$ .

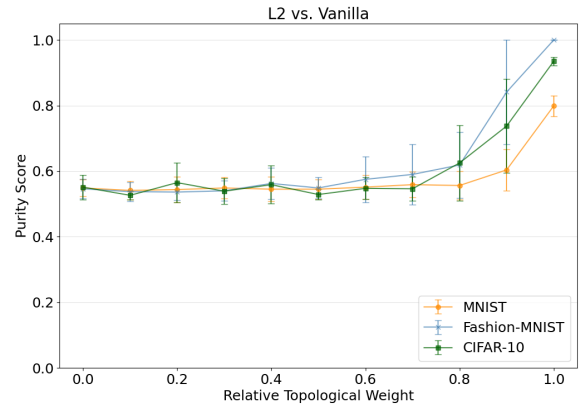


Figure 4: Purity scores of clustering connectomes of  $L^2$  and vanilla into two clusters with varying topological weight  $\lambda$ .

VGG and Resnet (He et al. 2016). For ResNet, we analyzed how different training strategies influence functional mechanisms in convolutional layers, which is similar to Study 1 in the main paper. We selected four ResNet-18 models via the timm library (Wightman, Touvron, and Jegou 2021). They were pre-trained on ImageNet using different training strategies and passed a random, stratified sample of 10,000 images of tiny-imagenet (Le and Yang 2015) through each model to construct a corresponding functional connectome. Similarly, we constructed 20 functional connectomes per pre-trained model, each based on a random sample of input data. Figure 5 presents the sample means of connectomes for each model across the 20 variations of input data. The distinct patterns in each model illustrates the differences in activation patterns produced by networks trained with different training strategies.

To further investigate the distinction, we employed the

same analysis pipeline based on persistence graph homology. For each pre-trained model, we obtained 20 functional connectomes and performed a clustering analysis across four groups. The Betti plots in Figure 6 visually represent persistence statistics extracted using various aggregation functions and layer depths. The detailed clustering performance reported in purity scores is summarized in Table 2. The distinct curves in the Betti plots and the high purity scores demonstrate that the proposed representation and analysis framework effectively captures certain aspects of the functional mechanisms within convolutional layers of modern architectures.

For VGG, we investigated how fully trained neural networks process different classes of stimuli in convolutional layers. We adopted the same architecture as the vanilla model used in our previous studies, consisting of three VGG blocks followed by fully connected layers. Similar to Study 2 in the main text, we examined how convolutional layers

|      | Early Layers      | Mid Layers        | Late Layers       |
|------|-------------------|-------------------|-------------------|
| Mean | $0.900 \pm 0.120$ | $0.875 \pm 0.168$ | $0.800 \pm 0.150$ |
| Max  | $0.825 \pm 0.160$ | $0.925 \pm 0.115$ | $0.912 \pm 0.119$ |

Table 2: Purity scores of clustering connectomes into four clusters corresponding to different training strategies of ResNet-18 models. The table compares results across different layer depths (columns) and aggregation functions (rows).

|      | Pearson           | Spearman          |
|------|-------------------|-------------------|
| Mean | $0.294 \pm 0.011$ | $0.201 \pm 0.009$ |
| Max  | $0.299 \pm 0.016$ | $0.218 \pm 0.013$ |

Table 3: Purity scores of clustering connectomes into 10 different clusters corresponding to classes in the CIFAR-10 dataset for a VGG-based model. The table compares results across different correlation measures (columns) and aggregation functions (rows).

process different stimuli. We obtained 20 functional connectomes per class and conducted a clustering analysis to group these 200 connectomes into 10 clusters. The detailed clustering performance in purity scores is summarized in Table 3. The purity scores, significantly above the expected 0.1, confirm that the proposed representation and analysis framework generalizes effectively to convolutional layers.

## Graph Theory Analysis

We employed graph theory properties to validate our representation of the neural network. To evaluate how the network is locally interconnected, we utilized the small-world coefficient. For a network to be considered “small-world,” it would have shortest path length between nodes, similar to a random graph, while also exhibit high local clustering of nodes. (Humphries and Gurney 2008)

With functional connectomes, the functional connectivity of a neural network can be represented as a complete graph. We computed the small world coefficients of the network at different edge densities by progressively removing edges based on their weights. First, we computed the clustering coefficient  $C$  and the shortest path length  $L$  of the graph. Next, we generated 10 random graphs with the same number of nodes and edges and calculated the corresponding metrics: the clustering coefficient  $C_{rand}$  and the shortest path length  $L_{rand}$ . Finally, the small world coefficient was determined as  $\frac{C/C_{rand}}{L/L_{rand}}$ . Averaged over 20 trials under the same setup as Study 1 in the main text, the small-world coefficient was computed and plotted with respect to edge density in Figure 7. Since all connectomes at various edge densities have a small-world coefficient greater than 1, this confirms that the graph representation of functional connectomes exhibits small-world properties.

Additionally, we explored a graph-theory-based approach for connectome analysis. Rather than performing clustering on the topological features of functional connectomes, we considered three graph-theory measures for the network: (1) weighted degree averaged across all nodes, (2) cluster-

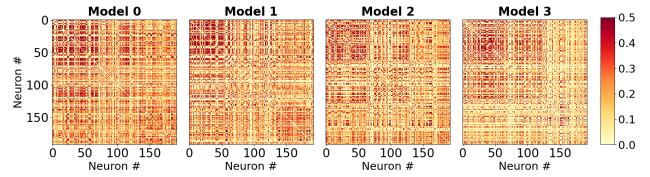


Figure 5: Sample means of functional connectomes, averaged within each of the four ResNet-18 models trained with different strategies.

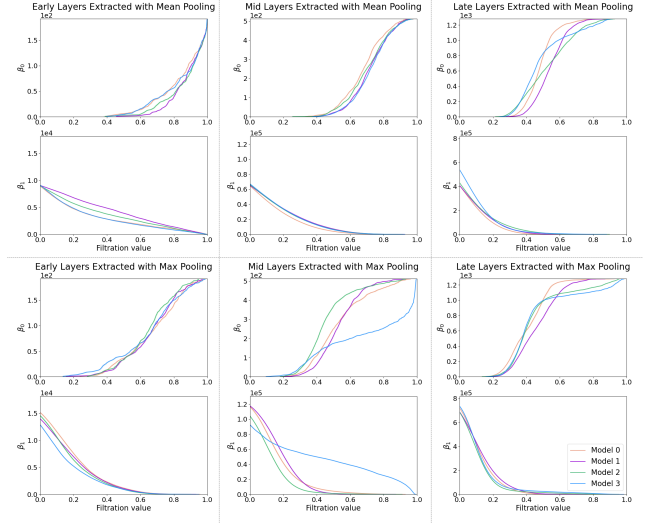


Figure 6: Persistence diagrams and statistics for each training strategy across different settings of layer depths (columns) and aggregation functions (rows). The thick lines represent Wasserstein barycenters, and the shaded regions indicate Wasserstein standard deviation.

ing coefficient averaged across all nodes, and (3) modularity. Using the same setup and connectomes from Study 1, we performed clustering on four groups comprising a total of 80 connectomes, corresponding to different regularization strategies used in training. The purity score, averaged over 20 clustering experiments, has a mean of 0.746 with a standard deviation of 0.006. This clustering performance, based on graph-theory features, is significantly higher than the expected 0.25, demonstrating the effectiveness of the representation.

## Dynamic Experiment

The dynamic experiment investigates changes in functional mechanisms during training. By recording the associated persistence statistics of functional mechanisms at different training stages, we are able to track the evolution in the topology of a network instance. For both 0D feature (connected components) and 1D feature (loops), we computed the change between training stages with 2-Wasserstein distance.

Specifically, we conducted a dynamic experiment with the same setup and hyperparameter settings as the experiment

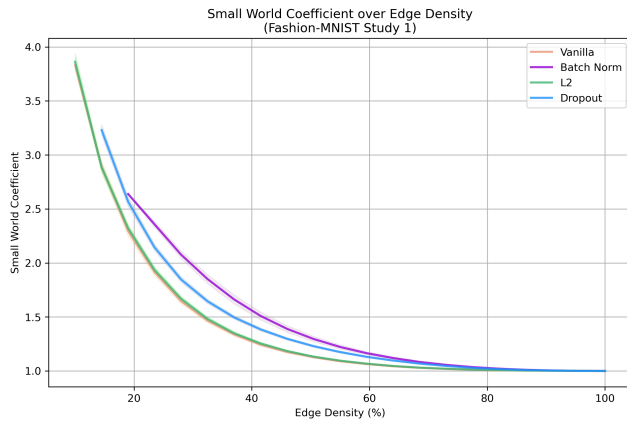


Figure 7: Small world coefficients of connectomes over various edge densities, compared across different regularization strategies. The thick lines represent mean small world coefficients of connectomes, and the shaded regions indicate standard deviation.

on the Fashion-MNIST dataset in Study 1 of the main text. In this experiment, we tracked both the changes in topology during training and the model’s classification performance. Since the model converges quickly, we adjusted the learning rate from 0.01 to 0.0005 to slow down convergence and plotted results from epochs 1 to 10 in batches. The batch size was set to 50 and there are 1200 batches per epoch. For every 60 batches, we recorded the state of the model and construct a corresponding functional connectome. This results in 20 functional connectomes captured sequentially per epoch for each model. Figure 8 shows the Wasserstein distance between consecutive functional connectome recordings for both 0D feature (birth of connected components) and 1D feature (death of loops). Figure 9 presents the corresponding training and testing accuracy over the same process. The experimental results are averaged over 20 trials.

The initial spike in the Wasserstein distance time series indicates that the functional mechanism is initially unstable. This appears to correspond with lower classification performance, as accuracy increases noticeably after stabilization. In addition, dropout exhibits a distinct pattern in its Wasserstein time series and accuracy over training compared to other regularization strategies. With higher classification performance, it also shows a much more pronounced initial jump and quicker stabilization of topology. This suggests that functional connectomes may reflect the model’s classification performance during training.

### Stability

We performed additional experiments using different randomization seeds. The results are consistent with our results and findings in the main text.

To verify the stability of our proposed functional connectomes, we injected Gaussian noise. In this experiment, we adopted the same architecture and hyperparameter settings as vanilla models trained on Fashion-MNIST in Study 1 of

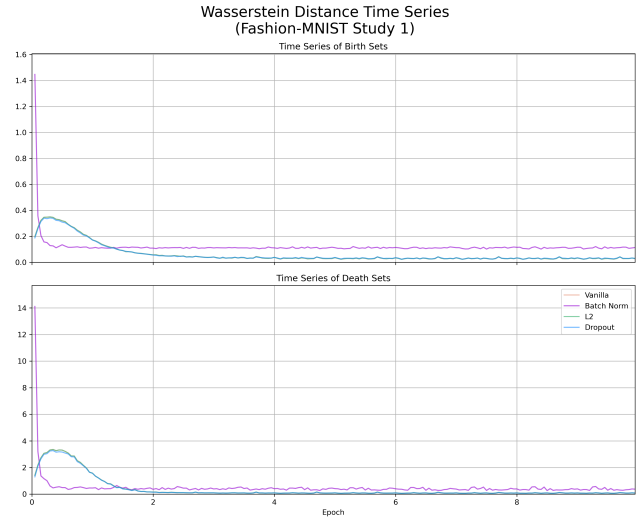


Figure 8: Time series of mean Wasserstein distance measured between consecutive recordings of connectomes across models with different regularization strategies. The top plot tracks changes in the 0D feature (connected components), and the bottom plot tracks changes in the 1D feature (loops).

the main paper. Gaussian noise  $\eta \sim \mathcal{N}(0, \sigma^2)$  was independently injected into the activation signal of each neuron. The connectomes were then constructed based on the Pearson correlation of the activation vectors. Finally, the clustering analysis was performed by grouping 80 functional connectomes according to the four regularization strategies used during training. The clustering performance was evaluated using the purity score.

In Figure 10, the clustering is repeated over 20 trials. The mean purity score is represented by the solid blue line and the shaded region indicates the standard deviation of purity scores. The steady decline in clustering performance demonstrates the robustness of our proposed representation against noise in the activation signal.

### Experimental Setup

The experiments were conducted on a MacBook Pro with an Apple M1 Pro chip and 16 GB of unified memory. The software environment was set up using the following configurations:

- **Operating System:** macOS Sonoma 14.5
- **Processor:** Apple M1 Pro
- **Memory:** 16 GB Unified Memory
- **Programming Language:** Python 3.11.9
- **Environment Manager:** Conda 24.1.2
- **Key Libraries:**
  - NumPy 1.26.4
  - Pandas 2.2.2
  - SciPy 1.13.0

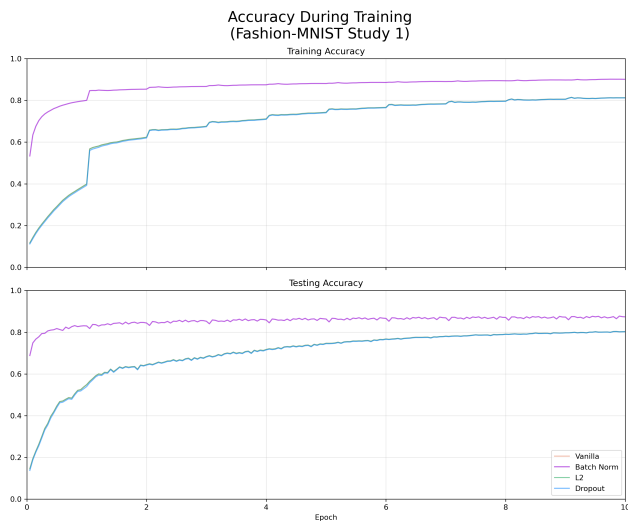


Figure 9: Time series of mean classification accuracy over recordings of accuracy scores across models with different regularization strategies. The top plot tracks changes in training accuracy, and the bottom plot tracks changes in testing accuracy.

- Matplotlib 3.9.0
- Scikit-learn 1.5.0
- Scikit-learn-extra 0.3.0.dev0
- Torch 2.3.0
- Torchvision 0.18.0
- Ripser 0.6.8
- Persim 0.3.5

All code was executed in a conda environment to ensure reproducibility. A seed value of 42 is used for randomization in `random` (Python), `numpy`, `torch`, and functions that accept a seed input.

## References

Adams, H.; Emerson, T.; Kirby, M.; Neville, R.; Peterson, C.; Shipman, P.; Chepushtanova, S.; Hanson, E.; Motta, F.; and Ziegelmeier, L. 2017. Persistence images: A stable vector representation of persistent homology. *Journal of Machine Learning Research*, 18(8): 1–35.

Carriere, M.; Cuturi, M.; and Oudot, S. 2017. Sliced Wasserstein kernel for persistence diagrams. In *International conference on machine learning*, 664–673. PMLR.

He, K.; Zhang, X.; Ren, S.; and Sun, J. 2016. Deep residual learning for image recognition. In *Proceedings of the IEEE conference on computer vision and pattern recognition*, 770–778.

Hoerl, A. E.; and Kennard, R. W. 1970. Ridge regression: Biased estimation for nonorthogonal problems. *Technometrics*, 12(1): 55–67.

Humphries, M. D.; and Gurney, K. 2008. Network ‘small-world-ness’: a quantitative method for determining canonical network equivalence. *PloS one*, 3(4): e0002051.

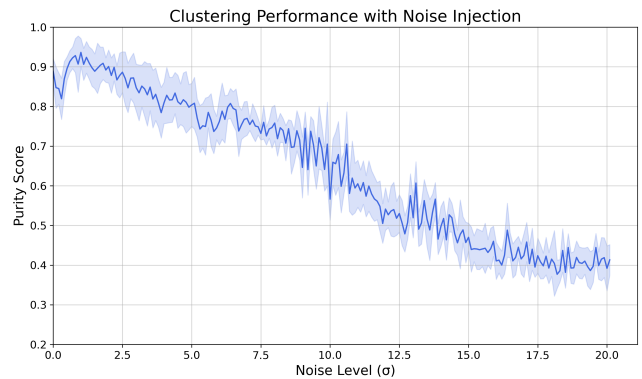


Figure 10: Purity scores of clustering connectomes with injected Gaussian noise across all regularization strategies into four clusters. The solid line represents the mean purity score over the standard deviation  $\sigma$  of noise injected, and the shaded region indicates the standard deviation of purity scores.

Ioffe, S.; and Szegedy, C. 2015. Batch normalization: Accelerating deep network training by reducing internal covariate shift. In *International conference on machine learning*, 448–456. pmlr.

Krizhevsky, A.; Hinton, G.; et al. 2009. Learning multiple layers of features from tiny images.

Le, Y.; and Yang, X. 2015. Tiny imagenet visual recognition challenge. *CS 231N*, 7(7): 3.

LeCun, Y.; Bottou, L.; Bengio, Y.; and Haffner, P. 1998. Gradient-based learning applied to document recognition. *Proceedings of the IEEE*, 86(11): 2278–2324.

Maas, A. L.; Hannun, A. Y.; Ng, A. Y.; et al. 2013. Rectifier nonlinearities improve neural network acoustic models. In *Proc. icml*, volume 30, 3. Atlanta, GA.

Manning, C. D.; Raghavan, P.; and Schütze, H. 2008. *Introduction to Information Retrieval*. Cambridge University Press.

Paszke, A.; Gross, S.; Massa, F.; Lerer, A.; Bradbury, J.; Chanan, G.; Killeen, T.; Lin, Z.; Gimelshein, N.; Antiga, L.; Desmaison, A.; Köpf, A.; Yang, E.; DeVito, Z.; Raison, M.; Tejani, A.; Chilamkurthy, S.; Steiner, B.; Fang, L.; Bai, J.; and Chintala, S. 2019. PyTorch: An Imperative Style, High-Performance Deep Learning Library. arXiv:1912.01703.

Pedregosa, F.; Varoquaux, G.; Gramfort, A.; Michel, V.; Thirion, B.; Grisel, O.; Blondel, M.; Prettenhofer, P.; Weiss, R.; Dubourg, V.; Vanderplas, J.; Passos, A.; Cournapeau, D.; Brucher, M.; Perrot, M.; and Duchesnay, E. 2011. Scikit-learn: Machine Learning in Python. *Journal of Machine Learning Research*, 12: 2825–2830.

Reininghaus, J.; Huber, S.; Bauer, U.; and Kwitt, R. 2015. A stable multi-scale kernel for topological machine learning. In *Proceedings of the IEEE conference on computer vision and pattern recognition*, 4741–4748.

Saul, N.; and Tralie, C. 2021. persim: A Python package for persistence diagrams and their similarity computations. <https://github.com/scikit-tda/persim>.

scikit-learn extra. 2020. scikit-learn-extra: a Python module for machine learning that extends scikit-learn.

Songdechakraiwt, T.; and Chung, M. K. 2023. Topological learning for brain networks. *The Annals of Applied Statistics*, 17(1): 403.

Songdechakraiwt, T.; Krause, B. M.; Banks, M. I.; Nourski, K. V.; and Veen, B. D. V. 2022. Fast topological clustering with Wasserstein distance. In *International Conference on Learning Representations (ICLR)*.

Srivastava, N.; Hinton, G.; Krizhevsky, A.; Sutskever, I.; and Salakhutdinov, R. 2014. Dropout: a simple way to prevent neural networks from overfitting. *The journal of machine learning research*, 15(1): 1929–1958.

TorchVision. 2016. TorchVision: PyTorch’s Computer Vision library. <https://github.com/pytorch/vision>.

Tralie, C.; Saul, N.; and Bar-On, R. 2018. Ripser.py: A Lean Persistent Homology Library for Python. *The Journal of Open Source Software*, 3(29): 925.

Wightman, R.; Touvron, H.; and Jegou, H. 2021. ResNet strikes back: An improved training procedure in timm. In *NeurIPS 2021 Workshop on ImageNet: Past, Present, and Future*.

Xiao, H.; Rasul, K.; and Vollgraf, R. 2017. Fashion-mnist: a novel image dataset for benchmarking machine learning algorithms. *arXiv preprint arXiv:1708.07747*.